Physical Science International Journal

25(4): 15-31, 2021; Article no.PSIJ.70903
ISSN: 2348-0130

Depth of Space and Radius of the Electron

Stefan von Weber[1] and Alexander von Eye[2*]

[1]Faculty Medical and Life Sciences, Furtwangen University, Jakob-Kienzle-Strasse 14, 78054 Villingen-Schwenningen, Germany.
[2]Department of Psychology, Michigan State University, 190 Allée du Nouveau Monde, 34000 Montpellier, France.

Authors' contributions

This work was carried out in collaboration between both authors. Author SVW wrote the first draft of the manuscript. Both authors together managed the literature search, the mathematical formulation and read and approved the final manuscript.

Article Information

DOI: 10.9734/PSIJ/2021/v25i430250
Editor(s):
(1) Dr. Volodymyr Krasnoholovets, Institute of Physics, National Academy of Sciences of Ukraine, Ukraine.
(2) Dr. Roberto Oscar, Aquilano National University of Rosario (UNR), Argentina.
Reviewers:
(1) Lucas Antonio Caritá, Brazil.
(2) Prasanta Bera, University of Southampton, U.K.
(3) Jie Fan, China.
(4) Shuyu CAI, Civil Aviation University of China, China.
(5) Yao FU, University of Chinese Academy of Sciences, China.
Complete Peer review History: https://www.sdiarticle4.com/review-history/70903

Original Research Article

Received 25 May 2021
Accepted 31 July 2021
Published 12 August 2021

ABSTRACT

The cosmological model of the expanding balloon in 4D-space (CM) delivers in interaction with a homogeneous vector field exactly Newton's law of gravitation with its 1/r-shape of the gravitational funnel. So far, the depth of space, *W*, in the 4-th spatial dimension can only be calculated using the theoretical approach of Feynman's radius of excess $r_{ex}=a/3$ with Schwarzschild-radius *a*. With this, the connection to the general theory of relativity (GR) is established, but the situation is unsatisfactory. In the present study, the possibilities of an experimental approach to the calculation of spatial depth, *W,* are explored. The only experimental approach so far is the bending of light on a central mass. We hypothesize in addition to the main effect $\varphi = -4a/y$, i.e., the angle of diffraction of a light beam on a heavy central mass in the distance *y* and with Schwarzschild-radius *a*, an additional effect close to the center of the form $\varphi_C \sim -1/y^4$. This additional effect has on the edge of the central mass about 1/3 of the strength of the main effect. However, its influence disappears very quickly with increasing distance. For this reason the sun cannot be used as the central mass. The bright corona and the strong magnetosphere do not allow measurements close to the sun.

**Corresponding author: E-mail: Stefan.vonWeber@hs-furtwangen.de, voneye@msu.edu;*

However, ESA's GAIA mission puts the planet Jupiter at the center of interest. This spacecraft measures with extremely high precision the positions of billions of stars. Results of first data analyses have already been published. As a side effect - the application of the CM to small particles provides an indication that the radius of the electron could be in the order of 10^{-23} m.

Keywords: Membrane; curvature; depth of space; gravitational funnel; radius of electron.

1. INTRODUCTION

„God has no origin and no end". This sentence of Christian Friedrich Gockel (1839) states one of the properties of our imagination of the hyperspace in which our universe expands besides countless other universes. The single universe may have an origin and an end, but not the hyperspace with its multiverses.

In a series of papers, [1-7], we proposed a cosmological model, the *Cosmic Membrane model* (CM), in which we use the frame of reference, σ_0, defined by the cosmic background radiation (CMBR), in the sense of an absolute 3D-space. A 4-dimensional balloon with a thin 3-dimensional envelope (membrane) expands in the 4D-hyperspace with an unknown speed of expansion, V_E. At the same time, a homogeneous vector field permeates the membrane perpendicularly. The membrane does not resist (or resists only marginally) if it is free of matter and tensed perpendicularly to the homogeneous vector field. However, when the membrane is charged with matter, it resists. The resistance produces a force that causes the curvature of the membrane (curvature of our 3D-space), and, as additional consequence, gravity and the effects of dark matter.

One can illustrate the origin of the homogeneous vector field by different physical phenomena, for example, a material flow reverse to the speed of expansion, or a material flow from the inside of the balloon, if one assumes over-pressure there. However, the origin of the homogeneous vector field can also be a form of radiation, or a completely new phenomenon. The authors hold back here, and enumerate here only some indispensable properties [3]. The following strong evidence speaks in support of the cosmic membrane model:

- The experimentally proven existence of the dipole-free frame of reference, σ_0. Therefore, the discovery of the CMBR by Wilson and Penzias [4] is one of the pillars of the CM.
- The result of the atomic-clock experiment of Haefele and Keating [3] can be explained much easier in the CM than in the SR. Therefore, the atomic-clock experiment is one of the key experiments of the CM, too.
- A 3D-membrane tensed in the 4D-hyperspace bends under central load as 1/r, which corresponds exactly to Newton's gravitational potential. For this reason, gravity simply becomes the downhill force, and becomes so explainable in a simple way [6].
- Another property of the membrane is that it clearly explains the decrease of the speed of light in a gravitational funnel, and it also explains in a simple manner light bending, radar echo delay, Einstein rings, and similar optical phenomena [3].
- Gravitational waves can appear in this cosmological model as well as longitudinal waves as in the form of transversal waves. The speed of the transversal waves still needs to be explicated.
- Another property of the curved membrane is the increased resistance. The increased resistance can explain the dark matter. Dark matter is, thus, a simple effect of the membrane which only arises together with the curvature of the membrane (curvature of the space), and therefore only in the neighborhood of real matter [2].
- The geodetic precession of a rotating body in the gravitational field can be explained by an increase in mass in the gravitational field together with the above-mentioned change in the speed of light in the gravitational funnel [4].
- Frame-dragging is conceivable in the CM, but not the Lense-Thirring effect. We have demonstrated [4] that the value of the Lense-Thirring effect found by the Gravity B Experiment is with high probability the geodetic precession of the gyroscopes in the gravitational field of the sun, caused by the absolute speed in the rest frame σ_0. Therefore, the Gravity B Experiment is also one of the key experiments of the CM.
- Because of the limited tension of the membrane of $F_o=2.164\times10^{19}$ [N/m^2] [2], neutron stars of the mass of the sun must

have a diameter of at least 200 km. A similar restriction for the minimal size or maximal mass also holds for black holes.

- The fact that the electrons orbit the atomic nuclei without fatigue since the big bang, or that light waves propagate without fatigue over billions of years through the space, is probably due to the influence of the homogeneous vector field. The homogeneous vector field submits nonstop huge amounts of energy to the matter embedded in the membrane.

Some newer considerations are:

- Because of the extremely high tension of the membrane of F_o=2.164×10^{19} [N/m^2] [2], one can conceive the stuff the membrane is made of only as a glassy, super strong material (for comparison: steel has a limit of about 10^9 [N/m^2]). Therefore, it is more likely that waves propagate instead of particles [6], or that the particles move outside the membrane, comparable to drops of water on a glowing hotplate, or comparable to drops of mercury on a marble top.
- There is strong evidence that leptons, i.e., electrons and positrons, consist of several charged building blocks. Electric charge means rotation of an object [8]. Here, vortexes of the homogeneous vector field can be conceived as a model of the CM. A single vortex filament stands perpendicularly on the membrane, and is in the 3D-space an electrically charged sphere with a rotating surface, but without a visible axis of rotation. The axis of rotation is directed toward the 4-th spatial dimension, i.e., it is inaccessible to us. In contrast, electrons and positrons have a spin and a magnetic momentum, which can be arbitrarily oriented in the space. From this fact follows that several electrical charged spheres rotate around each other. This way, the inner structure of electrons and positrons is comparable to the inner structure of baryons, for example, the proton.

2. DEPTH OF SPACE OF THE CURVED MEMBRANE

In [1], we have derived the ODE of the curved membrane under central load. In our cosmological model, the load from the 4th dimension is originated by the homogeneous vector field. This vector field reacts to disturbances in the membrane with a force in the direction of the negative w-axis. For example, matter embedded in the membrane is such a disturbance. The ODE is

$$w'' = -\frac{2w'}{r}. \tag{2.1}$$

Here, *w(r)* is the depth of space of the gravity funnel in the 4th spatial dimension, *w*, at a distance *r* from the center of mass of the central mass.

2.1 Calculation of the Depth of Space from Feynman's Radius of Excess

The depth of space, W_{0S}, at the edge of the sun, the tension F_0 of the membrane, and the vector-field acceleration A_V, which acts from the 4th spatial dimension on all matter inside the membrane, are essential constants of the CM. We have derived these constants from Feynman's radius of excess of the sun [9], r_{ex} = a/3, with the Schwarzschild radius

$$a = \gamma M_S / c^2 = 1.478.53 \text{ [m]}, \tag{2.2}$$

gravitational constant γ = 6.67422×10^{-11} [Nm^2/kg^2], solar mass $M_\odot$=1.991×10^{30} [kg] and speed of light c = 299,792,456 [m/s]. We equated Feynman's radius of excess, r_{ex}, with the path extension, *dS* [2], which occurs if one is approaching the edge of sun from infinite distance following the curved space of the gravity funnel (see Fig. 1).

Integration of the path and comparison of the path extension with Feynman's radius of excess, r_{ex}, results in Eq. (2.3).

$$W_{0S} = \sqrt{6 R_S r_{ex}} = 1.435\times10^6 \text{ [m]}. \tag{2.3}$$

Here, $R_S = R_\odot$ =6.956×10^8 [m] is the radius of sun. Newton's law of gravitation demands the curvature of space of the form *w(r)~1/r*. This condition for the curvature is fulfilled in a brane world with 4 spatial dimensions and a central load. The slope *w'(r)* of the membrane inside the gravitational funnel at the distance r ≥ R_S is given by Eq. (2.4).

$$w'(r) = \frac{W_{0S} R_S}{r^2}. \tag{2.4}$$

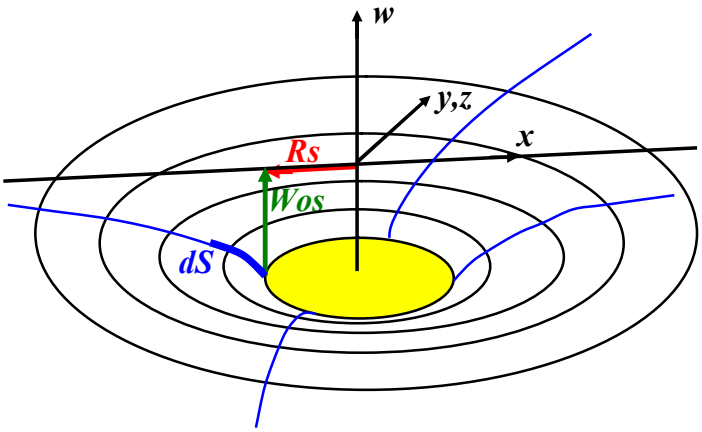

Fig. 1. Gravitational funnel and depth of space

The value of the slope *w'(r)* at the edge of sun is W'_{0S} = 2.06071×10^{-3}. In the CM, gravity is no direct force between two masses, but it is the downhill force. Here, the downhill force is the lateral component of the force the homogeneous vector field wields over the mass considered [1, 2]. This way, we have the connection to the gravitational acceleration $g_s = \gamma M_S / R_S^2$ = 274.04 [m/s^2] at the edge of sun. Backward, one can calculate the vector-field acceleration, A_V, by Eq. (2.5). $F_W = M A_V$ is the force the homogeneous vector field exerts on the mass M. Force F_W is directed to the negative w-axis.

$$A_V = \frac{g_s}{W'_{oS}} = 1.33\times10^5 \text{ [m/s}^2\text{]}. \qquad (2.5)$$

The vector-field acceleration A_V is a universal constant. The tension of the membrane, F_0, holds the mass M in the equilibrium against force F_W. Using the example of the sun, one can explain the calculation of tension F_0. The homogeneous vector field exercises the force $F_{WS} = M_S A_V$ on the mass of sun. From this relation, we obtain the tension $F_0 = M_S A_V / (4\pi R_S^2 w_{0s}')$. To obtain the small angle $\alpha = \arctan(w_{0s}')$ with the undisturbed membrane far away from the sun, we divide $M_S A_V$ by the slope w_{0s}' of the membrane at the edge of sun, because the sun does not make the membrane to be vertical. According to Eq. (2.4), we can replace w_{0s}' by W_{0S} / R_S, because, in the case of small slopes w' of the membrane, relation $w' = \tan(\alpha) \sim \sin(\alpha)$ holds. However, for greater values of w', we have to replace the slope $w' = W_{0S} / R_S$ by the expression $\sin(\arctan(w'))$. Using the data of the sun, we obtain, for the tension of the membrane,

$$F_0 = \frac{M_S A_V}{4\pi R_S^2 \sin(\arctan(W_{0S} / R_S))} = 2.11\times10^{19} \text{ [N/m}^2\text{]}. \qquad (2.6)$$

We assume, exept for changes in the vicinity of heavy masses, the tension F_0 is nearly constant for the whole universe. So, tension F_0 is another universal constant. If one wishes to calculate the depth of space, W_0, of other celestial bodies than the sun, for example for Jupiter or the Earth, one cannot use Eq. (2.3), because there the mean density of the sun is implicitly contained. Instead, one uses the escape energy $E_F = \gamma M / R$, which we set equal to the energy $E_W = W_0 A_V$. Here, E_W is the energy that is needed to lift an object of mass *1 kg* vertically over the distance W_0 against the force $F_{W1} = 1[kg]A_V$ of the homogeneous vector field. We find

$$W_0 = \frac{\gamma M}{R A_v}. \qquad (2.7)$$

For Earth, we find the depth of space at the surface of Earth as W_{0E} = 470.2 [m] calculated from mass M_E=5.975×10^{24} [kg] and radius R_E=6.378×10^6 [m]. For Jupiter, we find the depth of space at the surface of Jupiter as W_{0J} = 1.41906×10^4 [m] calculated from mass M_J=1.899×10^{27} [kg] and radius R_J=7.1398×10^7 [m].

The derivation of the depth of space W_{0S} at the edge of the sun from Feynaman's radius of excess of the sun is the connection of the CM with the GR. Theoretically, there exists another access to the estimation of the depth of space. This access is based on a small change of the

curved membrane near a great central mass, in addition to the 1/r-curvature. This small change could be measured by the bending of light or the delay of the runtime of radar echoes for sun-near trajectories of the beam.

2.2 Depth of Space W_{0S} at the Edge of Sun from the Shapiro Effect of Signal Retardation

We have published in [3] the derivation of the formula of the change of the speed of light inside the gravitational funnel. (see also Puthoff 2002 or Yarman et al. 2014 [10, 11]).

$$c(r) = c_{\ddot{o}}\left(1 - \frac{2a}{r}\right) \qquad (2.8)$$

The quantity c_o is the speed of light in vacuum for $r \to \infty$, $2a$ is the Schwarzschild radius of the Sun. The **Shapiro effect** of signal retardation by solar gravity is caused essentially by this decrease of speed of light $c(r)=c_o(1-2a/r)$ in the gravitational funnel. The decrease of speed of light is $v_d=2ca/r$, dependent on the distance r to sun. In 1977, Shapiro et al. [12] have measured the time delay of a radar signal travelling from the Earth to a planet (Venus, Mercury) and back with a sun-near trajectory. The authors used different frequencies to estimate and eliminate the influence of the corona of the sun.

The Cassini mission [13] had the main task of investigating and photographing the planet Saturn and his moon Titan. In addition, one important side effect of the mission was the opportunity to measure the signal retardation at a new level of accuracy. In 2003, Bertotti et. al. [14] published the results of this part of the experiment. The authors also used a range of frequencies to estimate and eliminate the influence of the corona of the Sun. We consider the light path in Fig.2, and use the labels used by Bertotti.

The signal starts from the Earth and travels to the Cassini orbiter. At the same time, the spacecraft sends signals with a constant frequency. Here, distance r_1 = 1 AU (AU = astronomical unit or length of the averaged great axis of the Earth's orbit) is the distance Earth-O, r_2 =8.43 AU the distance reflector-O. Distance ***b*** (the impact factor) is the nearest distance of the signal trajectory to the center of sun, i.e. the distance O-Sun. Integration of speed deficit v_d over the travel time (travel time of the signal at the path r_1 from Earth to point O) gives the path difference compared with a signal without speed deficit in the gravitational funnel. Now, x shall be the position on the path and r the distance between the position and the sun. We obtain with $dt=dx/c$ and $r^2= x^2+b^2$ after integration of $v_d=2ca/r$ the integral

$$dS = \int_0^{r1} 2ca/\sqrt{x^2+b^2}\,dx = 2ca\ \ln(r_1 + \sqrt{r_1^2+b^2}) - \ln(b)$$

[see, for example, Stoecker [15], integral 198]. Because the impact factor b is very small compared with the distance r, this reduces to $dS=2ca\ (ln(2r_1) - ln(b)$. So, we obtain the speed deficit equivalent extension of the path $dS_1=2a\ (ln\ (2r_1) - ln(b))$ or $dS_1=2a\ ln\ (2r_1/b)$ of the time delay. By the path O-reflector, we obtain $dS_2=2a\ (ln(2r_2) - ln(b))$ or $dS_2=2a\ ln\ (2r_2/b)$. By addition of dS_1 and dS_2, we obtain $dS_{12}=2a\ ln(\ (4r_1\ r_1\ )\ /\ (b^2)\ )$. Because each path is used twice, we need to double the amount, and obtain $dS=4a\ ln(\ (4\ r_1\ r_1\ )\ /\ (b^2)\ )$. From the equivalent path extension dS, we obtain by division with c, the speed of light, the time delay $d\tau$ of the round travel, e.g. Earth-Cassini-Earth, according to Eq. (2.9). Here, γ is the post-Newtonian metric parameter, which has in the GR the value of γ =1.

$$d\tau = \frac{2(1+\gamma)a}{c}\ln\left(\frac{4r_1 r_2}{b^2}\right), \qquad (2.9)$$

a result also given as Eq. (1) in [14]. The time retardation $d\tau$ is a positive value, i.e., the run-time τ of the radio signal increases by the value of $d\tau$. Because the distances r_1 and r_2 change

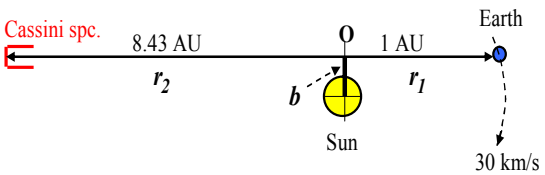

Fig. 2. Path of the radio signals from Earth to the Cassini orbiter and back

only unessentially during the few days of conjunction (Earth, Sun and spacecraft are on a line), the amount of the time delay $d\tau$ depends mainly on the impact factor ***b***. Our result, based on the CM formalism, agrees fully with the theoretical forecast of the GR.

Unfortunately, the *depth of space* W_o at the edge of sun cannot be derived from the effects of first order of light bending or signal retardation, because W_0 does not appear there. Therefore, we must consider effects of higher order in 1/b. Simulation calculations of a 3-dimensional membrane with a central load in the 4-dimensional space yielded the formula $dr/r=(1+w'^2)^{1/2}$ for the relative stretching dr/r of the membrane. This indicates that the membrane is stretched in radial direction inside the gravitational funnel. The tangential direction remains unchanged. The authors suppose now that this stretching of the membrane causes a relative *increase of the speed of light* according to $dc/c=1 + w'^2/2$. Another effect is the *geometrical path extension by the curvature* of the membrane in the gravitational funnel.

The Geometrical extension of the path is the sum of all differential extensions $dS=(dx^2+dw^2)^{1/2}-dx$. In the case of small slopes w' of the membrane, we find $dS=((dw/dx)^2/2)dx=(w'^2/2)dx$, or, from Eq. (2.4) the relation $dS=W_0^2R^2/(2x^4)dx$. This formula holds only for a trajectory through the center of sun. If the trajectory has the nearest distance y to the sun, then the relation $r^2=x^2+y^2$ holds, and, in addition, one must use the directional derivation $w`(x/r)$ instead of the radial derivation w'. Eq. (2.10) gives the signal retardation $d\tau_W$ of one part of the path (there or back). Fig. 3 shows the geometry.

$$d\tau_W = \frac{\Delta S_W}{c} = \int_{-\infty}^{\infty} \frac{W_o^2 R^2 x^2}{2cr^6} dx = \frac{\pi W_o^2 R^2}{16cy^3}. \quad (2.10)$$

The effect of the sun-near acceleration of speed of light $c_r(r)=c_o(1+w'^2/2)$ causes the distance gain dS_C per time unit dt. We find the relation $dS_C = (c\, w'^2/2)dt$. With $dt=dx/c$ and the directional derivation $w`(x/r)$, we obtain exactly the same integral as given in Eq. (2.10), but with the opposite sign. That means that the two sun-near effects cancel each other out, and we have no chance of finding the depth of space by the Shapiro effect.

The main effect according to Eq. (2.9) is predicted with exactly the same relation by the GR and the CM, but with slightly different theoretical foundations. This way, the experimental results of all Shapiro-effect missions confirm in the same way both theories, GR and CM, but cannot help to discriminate between GR and CM.

2.3 Depth of Space W_{0S} at the Edge of Sun from the Solar Gravitational Deflection of Light

The *light bending effect* $\varphi(y)= -2(1+\gamma)a/y$ (with $\gamma=1$ and y indicating the nearest distance of the trajectory of the beam to the sun) of the *solar gravitational deflection of light* is in the framework of CM caused by the common gravitation together with the effect of a decrease of the speed of light described above. The resulting formula is the same as given by the GR (cf. Weinberg [16], Premadi et al. [17], Bruckman & Esteban 1993 [18], and, in the case of strong gravitational fields, Puthoff [10]). Here, y is the nearest distance of the signal trajectory to the centre of the sun, with φ beeing the angle of deflection. In addition, we find three effects of the order $1/y^4$ in the framework of CM. The five effects of light deflection acting here are:

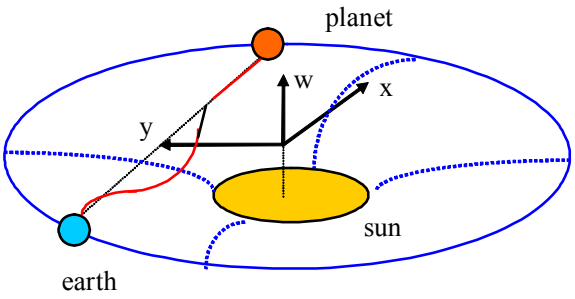

Fig. 3. Path extension in the x-w-plane

- G-effect or deflection caused by the y-component of **g**ravitation
- B-effect or deflection caused by a brake-effect of decrease of the speed of light inside the gravitational funnel and by the x-component of gravitation
- C-effect or deflection caused by a lateral effect of the centrifugal force in the x-w-plane
- P-effect or deflection caused by the y-gradient of the extension of the path
- A-effect or deflection caused by the sun-near acceleration of the speed of light

The G-effect: Common gravitational acceleration of the photon in y-direction is

$$A_y = -\left(\frac{\gamma M}{r^2}\right)\left(\frac{y}{r}\right) \qquad (2.11)$$

With $a = \gamma M/c^2$, $dx=dt/c$ und $r^2=x^2+y^2$ the integration over time (from -∞ to ∞) yields the lateral speed $v_y=-2ac/y$. By division with c, we obtain the result $\varphi_G= -2a/y$ or 0.875" as angle of deflection in the direction of the sun for a trajectory grazing the sun ($y=R$, R is here the radius of the sun). This value of 0.875 arcsec is one half of the main effect.

The B-effect: A photon is slowed down when entering the gravitational funnel. Fig. 4 shows the geometrical relations. Brake-acceleration is $A_b=dc/dt$. With $dx=dt/c$, $r^2=x^2+y^2$, $c\sim c_o$ and $c=c_o(1-2a/r)$ from Eq. (2.8), we find $A_b=2c^2ax/r^3$. The x-component of gravitation is $A_x = \left(-\gamma M/r^2\right)\left(x/r\right)$, and, with $a=\gamma M/c^2$, we obtain $A_x= -a\ c^2x/r^3$. The sum of both accelerations, $A_{bx}=c^2ax/r^3$, is negative at the entrance of the funnel (x<0), but positive at the exit. The y-gradient of this acceleration is $A_{bxy}=3c^2axy/r^5$ [(m/s²)/m]. Integration over $t=x/c$ (from $-\infty$ to ∞) yields the difference of the speed of two trajectories that are 1 meter apart. Further integration over $t=x/c$ yields the difference in path lengths at a given time and, thus, the angle of deflection φ_B according to Eq. (2.12).

$$\varphi_B = \int_{-\infty}^{\infty} -\frac{ay}{r^3}dx = -\frac{2a}{y}. \qquad (2.12)$$

Together, the G- and B-effects yield $\varphi=-4a/y$ as main effect, i.e., the same result as given by the GR.

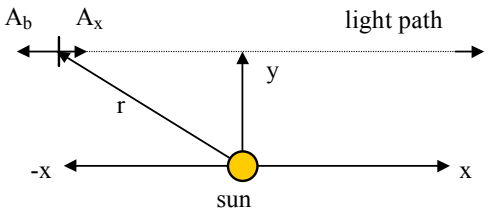

Fig. 4. Brake-force and x-gravitation inside the funnel

The C-effect is shown in Fig. 5. Here k is the radius of curvature of the trajectory with $\partial^2 w/\partial x^2 = 1/k$. Because, for positive second derivation of a curve $w(x)$, the acceleration vector points into the negative w-direction, the simple centrifugal acceleration is $A_C=-v^2/k$. With $\omega=v/k$, and $v=c$, we obtain $A_C=-\omega^2 k=-(c/k)^2 k=-c^2/k$. With $r^2=x^2+y^2$ and $w(r)=-W_oR/r$, we find $\partial w/\partial x = W_0 Rx/r^3$ and $\partial^2 w/\partial x^2 = (W_0R/r^3)-(3W_0Rx^2/r^5) = 1/k$. With $A_C=-c^2/k$, we obtain Eq. (2.13) for the centrifugal acceleration A_C.

$$A_C = \frac{3c^2W_oRx^2}{r^5} - \frac{c^2W_0R}{r^3}. \qquad (2.13)$$

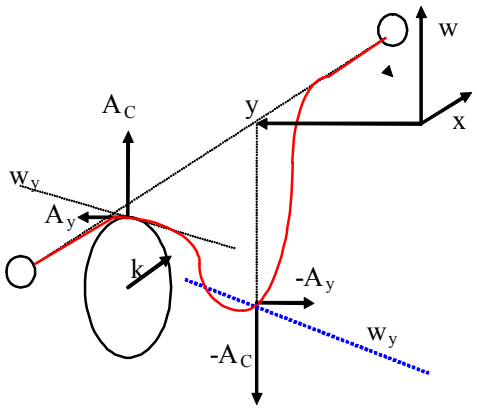

Fig. 5. Centrifugal acceleration A_C with lateral effect A_Y

The lateral motion, the effect A_C, is caused by the slope of the membrane $w_y = \partial w/\partial y$ with respect to the x-y-plane. A_C is exactly inside the x-w-plane. A_C is positive for large values of x. Inside the funnel, A_C is negative, and therefore, the component A_y is negative, too. With $r^2=x^2+y^2$,

the partial derivation $\partial w/\partial y = w_Y = W_0 R y/r^3$, lateral acceleration $A_Y = A_C w_Y$, speed $v_y = \int A_Y dt$, time unit $dt = dx/c$, and angle $\varphi_C = v_Y/c$, we find Eq. (2.14) for the deflection angle φ_C (see Stoecker integrals 84 and 95). The deflection angle φ_C is negative. This means that the trajectory is bent in the direction of the sun.

$$\varphi_C = \int_{-\infty}^{\infty} -W_o^2 R^2 y\left(\frac{1}{r^6} - \frac{3x^2}{r^8}\right)dx = -\frac{3W_o^2 R^2 \pi}{16 y^4} \quad (2.14)$$

The P-effect: To evaluate the P-effect, caused by the extension of the path inside the funnel, we start with the *y*-gradient of the differential path extension

$$\frac{\partial S}{\partial y} = \frac{\partial\left(\left(w'^2/2\right)dx\right)}{\partial y} = \frac{\partial\left(\left(\left(W_0^2 R^2\right)/\left(2\left(x^2+y^2\right)^2\right)\right)dx\right)}{\partial y} \quad (2.15)$$

resulting in

$$\frac{\partial S}{\partial y} = -\frac{2W_0^2 R^2 y}{r^3}. \quad (2.16)$$

By integration over *x* from $-\infty$ to ∞, one obtains a path difference and, therefore, the deflection angle

$$\varphi_P = -\frac{6\pi W_0^2 R^2}{8 y^4}. \quad (2.17)$$

The A-effect of central acceleration $c(r) = c_o(1 + w'^2/2)$ of the speed of light (caused by the stretching of the membrane inside the funnel) starts with acceleration of light $A_A = dc/dt$ and $dt = dx/c$. We find $A_A = -4c^2 W_o^2 R^2 x/(2r^6)$. Entering the funnel (x<0) A_A is positive, leaving it, A_A is negative. The *y*-gradient of A_A is $A_{Ay} = 12c^2 W_o^2 R^2 xy/r^8$. Twice integrated over $t = x/c$, we find the path difference of two paths that are 1 meter apart in y-direction at a given time, and, thus, the deflection angle

$$\varphi_A = \frac{6\pi W_0^2 R^2}{8 y^4}. \quad (2.18)$$

P-effect and A-effect cancel each other out. The only remaining effect of higher order is the lateral effect $\boldsymbol{\varphi_C}$ according to Eq. (2.14). In Fig. 6, one can see a well observable deviation in the light bending predicted by GR and CM in the range of 1<y<2.5 radii of the sun. Unfortunately, this range near the sun is the range of the corona. Measurement of light bending data is, here, charged with the unknown and quickly changing dispersion of the gaseous atmosphere of the surface of the sun. So, one must handle very cautiously all light bending data obtained in this range of radii.

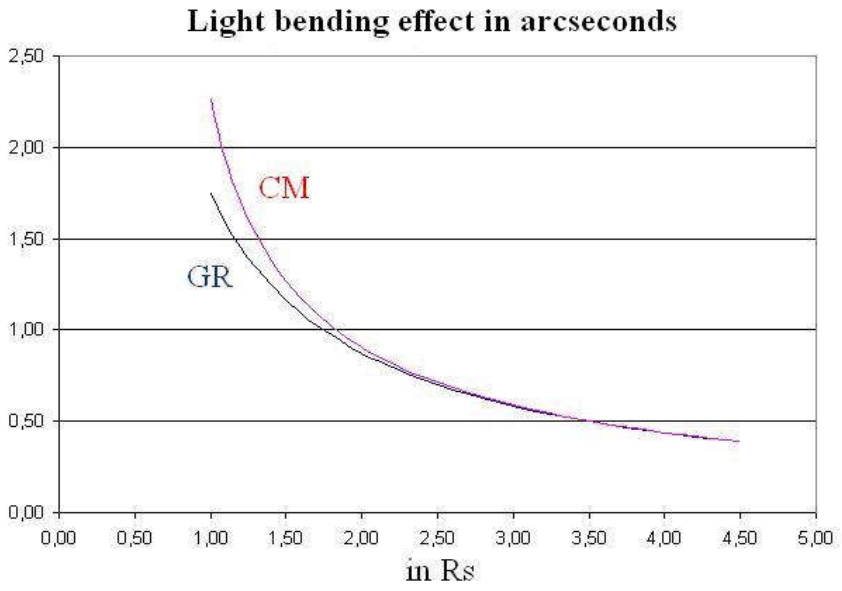

Fig. 6. Light bending near sun for GR and CM

3. DATA AND METHODS

3.1 Shapiro Effect of Signal Retardation

The experimental data by Shapiro et al. [12] from the Viking Relativity Experiment**,** in which radar pulses traveled between Earth and Mercury or Venus and back, confirmed the Shapiro-effect of signal retardation. The post-Newtonian term γ, which has the value of γ =1 in the GR, was determined by Shapiro et al. to γ =0.8±0.4. The influence of the solar corona was eliminated by Shapiro and his team using different wave lengths of the radar impulses. In 1979, Reasenberg, Shapiro et al. obtained, with better equipment for the round-trip times of light signals between Earth and Mars, a still improved result with γ =1.000±0.002.

Bertotti et al. [14] obtained in 2003 a still better result. Cassini-Huygens [13] was the mission of two coupled spacecrafts with the task of exploring the planet Saturn and his moon Titan. During summer 2002, the sun was positioned nearly exactly between Cassini-Huygens and the earth. It was a once in a lifetime opportunity to perform a new proof of the Shapiro effect. Similar to the method of Shapiro, the influence of the corona of the sun could largely be eliminated using different frequency bands. In 2003, Bertotti et al. [14] prepared the data in a complex procedure and published the scientific results. By their work, the Shapiro-effect was measured and confirmed with an accuracy never achieved before with γ =1.0000±0.0001. Because the effect is the same in GR and CM, it is also the same confirmation for both theories. Bertotti et al. not only confirmed the effect of signal retardation, but they could also exclude sun-near effects. This follows from the plot of the residuals after the fit of the observed data with the theoretical curve. Therefore, the Cassini-Huygens project is another important experiment, which puts the CM with an equal footing with the GR.

3.2 Solar Light Bending

In 1919, two expeditions were undertaken to Sobral and Principe to observe the solar eclipse with the aim to prove the General Relativity of Albert Einstein (1916). One of the initiators was A. S. Eddington [19]. Later it was said Dyson, Eddington and Davidson had only measured what they had wished to see, and moreover, the error of measurement had been greater than the effect they had sought. Other measurements confirmed Eddington, but showed also that an additional amount of light bending is possible and likely in the special case of sun-near trajectories, above the amount predicted by General Relativity.

Measurements of deflection angles of sun-near photon trajectories are only possible during eclipses of the sun. But there, an estimation of the influence of the solar corona is difficult to perform. Presumably, the dense atmosphere of the corona causes a deflection to the sun, too, but the sun wind, quantified by Fresnel's drag coefficient, causes a deflection away from the sun. Nevertheless, we use the data collected by Eddington in 1919 [19] and by van Bienstock in [20], given by Weinberg [16], Mattig [21], and Schmutzer [22]. Some of the data were the same. Table 1 gives light bending data from 12 eclipses. Col. 1 indicates the site and col. 2 the year of the eclipse. Col. 3 gives the bending angle in arcsec for a distance of $r = R_S$, col. 4 the estimated error in arcsec. Col. 5 shows the references.

Table 1. Light bending data from 12 eclipses between 1919 and 1952

Place	Year	Angle in ´´	Error in ´´	Source
Sobral	1919	1,98	0,17	Dyson et al.
Principe	1919	1,61	0,45	Dyson et al.
Takegon	1929	2,24	0,10	Schmutzer
Australia	1922	1,61	0,40	Weinberg
Australia	1922	1,77	0,40	Weinberg
Australia	1922	1,79	0,19	Weinberg
Australia	1922	1,72	0,15	Weinberg
Australia	1922	1,82	0,20	Weinberg
USSR	1936	2,73	0,31	Weinberg
Japan	1936	1,7	0,21	Weinberg
Brazil	1947	2,01	0,27	Weinberg
Sudan	1952	1,7	0,10	Bienstock

To obtain a mean value, we weighted the angles with the square of their inverse standard error, and so we obtained the mean deflection angle of φ = 1.91'' ± 0.19'' of the above 12 eclipses of the sun. The error of ±0.19'' is the harmonic average of the single errors. GR predicts φ=4a/R=1.75'' for trajectories grazing the sun. We take the difference (1,91±0.19)''-1,75''=(0.16±0.19)'' and compare it with the result of Eq. (2. 4). Thus, we obtain with $y=R_S$ another estimate of the depth of space with W_{0S} = (2,04 ± 2,2) ×10^5 [m]. This value is only 1/7-th of our theoretical value of W_{0S} = 1,435 ×10^6 [m]. Otherwise, the uncertainty of the estimated value is large. But the observations of Robertson und Carter 1984 [23] show also an increase of the deflection angles for sun-near signal trajectories. Otherwise, in 2009, Formalont et al. [24] did not find any additional near-sun effect. Their very precise measures, based on the VBLA-method, of the deflection of cosmic radio waves gave a limitation to the interval γ=1.0000 ± 0.0003 of the post-Newtonian parameter γ. They used the strong radio source 3C273, and they measured with a precision of 0,01 mas (milliarcseconds) the distances to several fainter radio sources more distant from the orbit of the sun. But Formalont et al. also noticed in their paper that, for a trajectory nearer than ~3° to the sun, all measures were unusable. The distance of 3° corresponds roughly to 12 radii of the sun. So, there was never a chance to find our assumed sun-near effect.

In 1989-1993, the satellite HIPPARCOS measured the positions of numerous stars under different positions of the sun several times, with a precision of only a few mas. The evaluation and the comparison of the positions yielded another convincing proof of the main effect of gravitational light bending. The relation $\varphi(y)= -4a/y$ has been proven anew with high accuracy. Otherwise, because of the danger of destruction of the optical arrangement by direct sunlight, the measurements ended at an angle of 45° to the sun. Our hypothesized sun-near effect falls below the mas-limit for a distance smaller than 1.6°. This angle is equivalent to about 6 radii of the sun. Therefore, all these measures of the satellite HIPPARCOS make no contribution for a decision pro or against CM, because the main effect is identical in both theories.

In 2013, the GAIA-mission was started by the ESA [25]. Since 2013, this satellite measures with a precision about 200-fold higher than that of HIPPARCOS the 10,000-fold number of stars. The mission was extended only recently until 2025. Until now, the data of 4.6 billion objects have been published in 3 catalogues. Numerous researchers have recognized early on the possibility to study relativistic effects of the bending of light, especially by the influence of the planet Jupiter. So far, however, no evaluations have been published on the topic of light bending by Jupiter. Similar to the HIPPARCOS-mission, the GAIA-mission avoids sun-near star positions. Also, bright fixed stars and large planets cannot be measured by the GAIA spacecraft. This means that it is very hard for astronomers and astro-physicians to obtain proper data. The beginning has been made, e.g. by Abbas et al. in 2018 [26].

3.3 Jovian Light Bending and Time Delay

Jupiter is the greatest planet of our solar system. Its mass is about 1/1000 of the mass of the sun, and its diameter about 1/100 of the diameter of the sun. The surface of the planet is cold and so it has no sun-like corona. Light grazing the edge of the Jupiter is expected to be deflected by an angle of about 17 mas. This angle is large enough to be detectable.

In 2003, Formalont et al. **[**27] determined the relativistic influence of the planet Jupiter as it passed in a small distance (3.7' ~14 Jovian radii) the trajectory of the radio waves of the quasar J0842+1835 on September 8, 2002, by measuring the time delay using the VLBA-method. At closest approach (3.7'), General Relativity (GR) predicts a radial (static) deflection of 1190 *μ*arcsec, and a tangential (retarded) deflection in the direction of Jupiter's motion of 51 *μ*arcsec. The tangential (retarded) deflection relates to the speed of gravity, c_g. The experiment achieved a rms position error of ≤10 *μ*arcsec, and measured the retarded deflection to be 0.98± 0.19 (rms error) times the value that is predicted by the GR. The GR predicts that the constant c_g equals the speed of light *c*. The experiment measures the numerical value of c_g as a test of the Lorentz invariance of the Einstein equations, and is an indirect measurement of the speed of propagation of gravity.

However, the nearest distance between the orbit of the Jupiter and the trajectory of the radio waves of the quasar was 14 times the Jovian radius, much too far to detect effects of order $1/y^4$. The main effect of light bending is about φ_{GR}=16500 μas for a beam grazing the surface of Jupiter. The additional surface-near effect

supposed by the CM is about φ_{CM}=4800 µas for the same beam. But, for a trajectory with the nearest point at r/R_J =14, the main effect is φ_{GR}=1190 µas, but only φ_{CM} =0,125 µas for the additional surface-near effect supposed by the CM and the same beam. This is a reduction from 29% to 0,01% for the ratio φ_{CM} / φ_{GR}. Thus, there was no chance to detect deviations between GR and CM.

The Jovian magnetosphere also produces a radial deflection of the radio waves, in the opposite direction of the gravitational radial deflection of light. However, calculations suggested that this bending would be significantly less than the small, retarded deflection term of 51 µarcsec, i.e., about 5 µarcsec. This way, the influence of the magnetosphere will not essentially disturb the measurements of the deflection of light according to the main effect and the additional surface-near effect supposed by the CM.

3.4 Reanalysis of the Light Bending Data of Eddington

We re-analyzed the Eddington data from 1919 [19]. Fig. 7 shows the bending angles of the seven stars measured by Eddington et.al. The black line is the prediction of the GR and of the main effect of the CM, i.e., in both cases $\varphi(r)=1.75''/r$. Here, r is the dimensionless ratio "distance r / radius of sun". The pink line is the prediction of the CM, i.e., the GR prediction with an additional sun-near term as $\varphi(r)= 1.75''/r + 0.514''/r^4$. The number 0.514'' is computed using Eq. (2.14) with the theoretical depth of space $W_{0S} = \sqrt{6 R_S r_{ex}}$ = 1.435×10^6 [m] at the edge of the sun. Both curves, GR and CM, remain below the bending angles of the three nearest stars. The green curve, labeled by EXP, shows the result of the non-linear regression with the model $\varphi(r)= 1.75''/r + b_1 e^{-b2\, r}$. The exponential function was chosen by us as a first approach of the density curve of the corona of the sun. The coefficient b_1 was estimated to be b_1 = 0.696''± 0.32'', the coefficient b_2 as b_2 = 0.956. The blue curve, labeled with "1/r^4", shows the result of the non-linear regression with the CM-model $\varphi(r)= 1.75''/r + b_3 / r^4$, but with a fitted value of the additional effect. The coefficient b_3 was estimated to be b_3 = 1.70''± 0.79''. The errors of the coefficients of both nonlinear regressions, b_1 and b_3, are large. The t-value of the EXP-fit is t_{EXP}=2.18 with 5 degrees of freedom, and the t-value of the 1/r^4-fit is $t_{1/r4}$=2.16 with 6 degrees of freedom. Both t-values are not significant using the 5%-level of significance. The data and the calculated points of the four curves are shown in Table 2. The two curves named as GR and CM are predictions. The two curves named as EXP and 1/r^4 are fitted curves.

Fig. 7 shows the 7 data points measured by Dyson et al. together with the four fitted models.

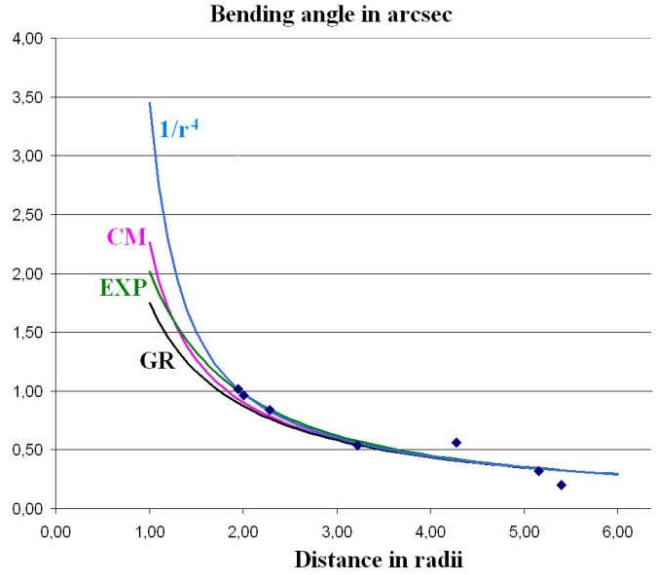

Fig. 7. Comparison of 4 light bending models

Table 2. Light bending data of Dyson et al. with two predictions and two fitted models

r	φ	GR	CM	EXP	$1/r^4$
1,00		1,75	2,26	2,02	3,45
1,50		1,17	1,27	1,33	1,50
1,95	1,02	0,90	0,93	1,01	1,02
2,01	0,97	0,87	0,90	0,97	0,98
2,28	0,84	0,77	0,79	0,85	0,83
3,22	0,54	0,54	0,55	0,58	0,56
4,27	0,56	0,41	0,41	0,42	0,41
5,15	0,32	0,34	0,34	0,34	0,34
5,40	0,20	0,32	0,32	0,33	0,33

One can measure the averaged distance of the 4 curves to the given n=7 data points by the resting standard deviation s_r. The obtained values are $s_{r,GR}$=0,0951'', $s_{r,CM}$=0,0874'', $s_{r,EXP}$=0,0786'', and $s_{r,1/r4}$=0,0789''. How one can see – the predicted curves have greater values of the resting standard deviation s_r than the fitted curves. The CM-prediction is a little better, but without significance by a F-Test. As one can see immediately, all models can hardly be distinguished within the range $r>3R_S$ of radii. The great uncertainty begins for radii $r<3R_S$. Therefore, we performed two simple simulation experiments.

With the first experiment, we tried to find differences in the results from the two methods of analyzing the light bending data, given in the literature, e.g., in [19, 20].

1. Method 1 is the **curve fit** with the adequate regression model $\varphi(r)=b''/r_i + e_i$ over all measures (φ_i , r_i) of one eclipse. The coefficient *b* estimates the expected effect $\varphi(r)$ for *r=1* (i.e., at the border of the sun). This method was used by Dyson et al. [19].
2. Method 2 involves **averaging**. This means that the formula $\Phi_i = \varphi_i \, r_i$ estimates the expected effect Φ_i for *r=1* (i.e., at the border of the sun) individually for each star. Then, all Φ_i-values are averaged. This method was used by van Bienstock [20].

In a first step, we extracted 11 typical radii from the data of Dyson et al. [19], van Bienstock [20], and Mattig [21]: (r_i = 1.9, 2.1, 2.3, 2.7, 3.2, 3.7, 4.3, 4.8, 5.3, 5.8, 6.5).

The model of the main effect of light bending by a spherical mass has both in the GR (see [16]) of A. Einstein and in the CM (see chapter 2, *G*- and *B-effect*) the same form. It is $\varphi(r)=4a/r=1.75''/r$ with Schwarzschild-radius *a.* Here, the quantity *r* is the dimensionless ratio of the nearest distance of the trajectory *y* to the center of mass and the radius *R* of the central mass. The value $\varphi(r=1)=1.75''$ corresponds to the light bending by the sun. We produced 12 data sets (corresponding to 12 eclipses) each with 11 random data pairs (φ_i , r_i) (corresponding to 11 stars pro eclipse) using the formula $\varphi(r_i)=1.75''/ r_i + E \cdot Rand.$ Here, *Rand* is a normally distributed random number N(0;1), and *E*=0.1'' the standard deviation for the angle $\varphi(r_i)$ of light bending of a single star. Then we evaluated the 12 random data sets using the two above-described methods without any change in the data. Table 3 shows the results.

Method 1 *(curve fit*) produces the most stable estimation. The standard deviation for method 2 (*averaging*) with a value of σ =0.117 is significantly greater than σ =0.069 for method 1 *(curve fit*). The maximum difference in the estimation of $\varphi(r=1)$ was 0,2'' in our simulation. However, the mean values of the 12 eclipses hardly differ. This way, the comparison of the two data analysis methods shows no significant difference. In practice, it does not matter which method is used.

Table 3. Comparison of two methods of estimation of $\varphi(r=1)$

E=0.1''	*Curve fit*	*Averaging*	*Difference*
Mean	1.775	1.760	0.014
Maximum	1.932	2.006	0.202
Minimum	1.684	1.598	-0.107
Stand.dev.	0.069	0.117	0.102

Table 4. Curve fit with the GR-model for GR-modeled and CM-modeled data

E=0.1''	$\varphi_{GR}(r=1)$	$\varphi_{CM}(r=1)$	Difference
Mean	1.732	1.761	-0.029
Maximum	1.936	1.974	0.290
Minimum	1.569	1.553	-0.236
Std.dev.	0.130	0.123	0.132

The CM not only predicts the main effect, $\varphi(r)=4a/r=1.75''/r$, which is in the GR and CM identical, but also the additional effect according to Eq. (2.14). In the case of light bending by the sun, we obtain together with the main effect the model $\varphi_{CM}(r_i)=1.75''/ r_i + 0.514''/ r_i^4$. With the second simulation experiment, we tried to find the influence of an inadequate regression model on the result $\varphi(r=1)$. Here, we produced two different data sets: (1) using the GR-model $\varphi_{GR}(r_i)=1.75''/ r_i +E\cdot Rand_1$, and (2) using the CM-model $\varphi_{CM}(r_i)=1.75''/ r_i + 0{,}514''/ r_i^4 + E\cdot Rand_2$. Here, $Rand_1$ and $Rand_2$ are stochastically independent random numbers both of type N(0;1). Also, here the index i ran from 1 to 11, and we performed 12 repetitions (according 12 eclipses). Each data set with its 11 data pairs, independent of its different origin, was fitted with the same regression model $\varphi(r)=b''/ r_i + e_i$. For the CM-modeled data, the model was inadequate. Table 4 shows the results.

The comparison of the simulation results shows that there are no significant differences. The evaluation of the CM-modeled data with the false regression model is not noticeably worse, or, with other words, the hypothesized sun-near effect cannot be proven with such imprecise light bending data.

4. RADIUS OF THE ELECTRON

The classical electron radius R_e has been estimated already shortly after the discovery of the electron. One obtained the estimation of R_e from the doubled electrostatic self energy of the charge of the electron which has been equalized with the energy of the mass equivalent of the electron. Here, one thinks that the charge is evenly distributed on the surface of a ball. R_e has been calculated as $R_{e,classic}=2.8179\times10^{-15}$ [m]. In 2020, Salah Eid [28] calculated the electron radius from the energy of the gamma quant (according to Bethe's experiment in 1938) which can split the deuterium nucleus into a neutron and a proton. He assumes that the gamma quant is constructed by an electron-positron couple circling each other touching each other. He calculated R_e as $R_{e,Salah}=3.623\times10^{-16}$ [m]. In 2014, the Chinese Particle Data Group [29] published that the electric dipole moment of the electron has the limit $d<10.5\times10^{-28}$ [e cm], but it published no radius. In contrast to the electron, the same group publishes for the proton several radii, depending on the property that the radius is supposed to describe, with values between $R_p=0.77\times10^{-15}$ and $R_p=0.87\times10^{-15}$ [m]. This corresponds to the opinion of many researchers that the electron is point-shaped, i.e., without expansion and, therefore, $R_e=0$. This opinion is also supported by the fact that, for example, experiments at CERN showed that the radius $\boldsymbol{R_e}$ of the electron must be smaller than 10^{-19} [m] [30]. We do not think that's a proof for $R_e=0$, however. We already mentioned one argument in the introduction: The electron consists of several charged building blocks, i.e., a structure similar to the quarks in the proton.

According to CM, the electron sinks into the membrane according to its mass, and produces a small gravitational funnel. We assume that the tension F_0 of the membrane is constant for the entire membrane, with the exception of small changes near heavy masses. To obtain an estimate of the radius $\boldsymbol{R_e}$ of the electron, we posit that the relation $\boldsymbol{R_e} = \boldsymbol{W_{0e}}$ holds, i.e., the depth of space at the edge of the electron equals the radius $\boldsymbol{R_e}$. We use, according to Eq. (2.7), the two potential energies: (1) $E_1 = W_0\ A_V$, i.e., the energy needed to lift the mass of 1 kg over the distance W_0 against the acceleration A_V, and (2) $E_2 = \gamma\ M_e / R_e$, i.e., the energy needed to lift the mass of 1 kg in the potential field of the electron from distance R_e to the distance of $r \rightarrow \infty$. With $E_1 = E_2$ and $\boldsymbol{R_e} = \boldsymbol{W_{0e}}$, we obtain the relation

$$R_e = \sqrt{\frac{\gamma\ M_e}{A_V}}\ . \qquad (4.1)$$

The numerical value of $\boldsymbol{R_e}$ is $\boldsymbol{R_e} = \boldsymbol{W_o} = 2.14\times10^{-23}$ [m] calculated with gravitational constant $\gamma=6.674\times10^{-11}$ [Nm^2/kg^2], mass of electron $M_e=9.104\times10^{-31}$, and vector-field acceleration $A_V=1.33\times10^5$ [m/s^2]. For comparison, a number of experiments results in $\boldsymbol{R_e} < 10^{-19}$ [m]. The Planck length $\boldsymbol{l_p}$ is given with $l_p = 1.616\times10^{-35}$ [m].

Our estimation of R_e = 2.14×10^{-23} [m] fits in well. Accordingly, the radii of the charged building blocks of the leptons (the rotating charged spheres supposed by us) must still be much smaller.

Our condition for the estimation, $R_e = W_{0e}$, is chosen arbitrarily. However, we made that decision, because the membrane has already the slope $w'(R_e)=1$ at this point, and the slope will rapidly increase on further approach to the center. Probably, one will find no exact radius of the electron, similarly, just as in the case of the proton. Another problem is the relativistic contraction of moving particles. The SR assumes a length contraction in the direction of movement using the relation $x' = x\sqrt{1-\beta^2}$ with $\beta=v/c$. The CM assumes length contraction and cross contraction with the relation $x' = x\left(1-\beta^2\right)$, and $y' = y\sqrt{1-\beta^2}$, respectively. An electron with a speed of 99% of the speed of light shortens its lengths in the direction of movement to 2% of its original length of 2 R_e, and it shortens its width to about 15% of its original width of likewise 2 R_e. This example shows that scattering experiments with high-energy electrons do not measure the true size of the electron.

5. RESULTS AND DISCUSSION

The GR knows three spatial dimensions and the time as fourth dimension. Therefore, the depth of space plays no role in the cosmological model. In contrast, the CM works with four spatial dimensions. Our 3-dimensional space is the thin membrane of a 4-dimensional balloon. The membrane may have a curvature with hills and dales in the fourth dimension. Depth of space is the depth of such a dale. Therefore, a big goal is to find an experimental access to the spatial depth, *W*, in the gravitational funnel of a central mass. So far, there exists only the theoretical approach with Feynman' radius of excess rex = a/3 with the Schwarzschild radius a = γ M_S / c^2. We have shown as our contribution to this issue of research that there could be the experimental approach. Gravitational light bending from a heavy mass is a hot candidate. We hypothesize, beside the known main effect, which is in GR and CM the same, an additional effect close to the center that, close to the center, increases the deflection angle of a light beam even more. The main effect's light deflection, $\varphi = -4a/y$, has two reasons: (1) ordinary gravitation deflects the light quanta towards the central mass, and (2) the decrease of the speed of light in the gravitational funnel that causes a small deflection of the wave fronts. Otherwise, our hypothesized additional effect, $\varphi_C \sim -1/y^4$, depends on the square of the depths of space, i.e., W^2, according to Eq. (2.14), and has the distance statistics $1/r^4$. Shapiro's effect of time retardation when a signal passes through the gravity funnel does not show a dependence upon the depth of space *W*. It is therefore of no interest for this special purpose.

So, our central interest focuses on the relativistic diffraction of light. An inspection of the many experiments and observations on the diffraction of light on the sun and the planet Jupiter, results in the following view:

Most near-sun trajectories of light beams, which can be measured by the position shifts of the stars, end at a distance of about 2 $R_\odot$ from the center of the sun, as seen in Eddington's data [19]. The corona of the sun, which is already visible to the naked eye during an eclipse, extends to three $R_\odot$. The invisible magnetosphere presumably extends much further. Accordingly, diffraction measurements below 3 solar radii are definitely incorrect, and they are useless as evidence of a sun-near additional effect, because the value of this effect has decreased to 1/81st of its original value, which it has for $r=R_\odot$. Even the highly precise measurements using VLBA do not change anything (e.g., Formalont et al. in 2009 [24]) – to the contrary, they end at a distance of 12 $R_\odot$. The sun is, therefore, not a suitable research object when it comes to the spatial depth of space *W* of the gravitational funnel.

In contrast, Jupiter has only 1/1000-th of the mass of sun, but also only 1/10-th of the sun's diameter. Therefore, the relativistic light bending is 100 times smaller in relation to the sun, but its value is large enough to be measured very precisely. Thanks to GAIA, one can measure the positions of the stars with a precision of only some few µas. This position seems to be changing, when the planet Jupiter approaches the light path star-Earth. Unfortunately, bright stars - and the planet Jupiter is very bright – cannot be measured by GAIA. Therefore, it is a complex procedure to extract the correct positions of the stars from GAIA's data catalogues with and without the influence of the giant planet. Specifically, a time lag arises, because, to obtain clean comparison positions the planet has to move far enough from a chosen

position at the sky. Because of the time lag, one must also pay attention to the proper motions of the stars, the changed parallaxes, and the ubiquitous diffraction influence of the sun. This is a job for astronomers and astrophysicists with experience concerning the GAIA mission and its data catalogues. The first evaluations of data are already in progress, e.g., by Abbas et al. [26]. Initially, however, it was a question of the accuracy that can be achieved.

The Jupiter has no corona, but a magnetosphere [31]. The magnetosphere of Jupiter is dominated by the rotation of the planet that spins with a 10 h rotation period. For example, the satellite Io loses ~1 t/s of atmospheric material that becomes trapped in Jupiter's magnetic field. The densest plasma forms a torus around Jupiter just outside the orbit of Io. However, in 2003, Formalont et al. [27] have determined the density and the course of the density of the magnetosphere of the Jupiter. The Jovian magnetosphere also produces a radial deflection of radio waves, which goes in the opposite direction to the gravitational radial deflection of light. However, calculations suggested that this bending would be significantly less than the small, retarded deflection term of 51 *μ*arcsec, i.e., about 5 *μ*arcsec. This way, the influence of the magnetosphere will not essentially disturb the measurements of the deflection of light that is caused by the main effect and the additional near-surface effect posited by the CM. Here, we see an opportunity to confirm our assumption in the near future.

Summarizing the results of this paper concerning the determination of the depth of space, we can exclude light bending by the sun, caused by its strong corona, as an experimental base. There is a lot of literature and a lot of experimental data [11, 13, 14, 16, 19, 20, 21, 23, 24] on the diffraction of light on massive objects, but none for trajectories of the diffracted light rays close to the center. However, due to the lack of corona, diffraction of light by the planet Jupiter could become the center of attention in the near future [27], despite its strong and extensive magnetosphere [31].

Electrons have a spin axis which can - in absence of magnetic fields – point into arbitrary directions. An electric charge can be explained by rotation (see, for example, Mueller [8]). Here, under the paradigm of the membrane, vortexes of the homogeneous vector field are a conceivable model. A single vortex filament stands perpendicularly on the membrane, and is, in the 3D-space, an *electrically charged sphere* with a rotating surface, but without a visible axis of rotation. The axis of rotation points into the 4-th spatial dimension, i.e., it is inaccessible to us. Otherwise, electrons and positrons have a measurable spin, as above noted, and a magnetic momentum, which can be arbitrarily oriented in space. From this fact follows that several electrically charged spheres must rotate around each other. This way, the inner structure of electrons and positrons is comparable with the inner structure of baryons, for example the proton.

Experiments showed that the electron must be smaller than 10^{-19} m. As a particle with mass, it produces a small gravitational funnel with a computable shape. Now, we postulated the radius $\boldsymbol{R_e}$ of the electron so that it equals the depth of space, $\boldsymbol{W_{0e}}$, at the edge of the electron. The numerical value found by us is $\boldsymbol{R_e} = 2.14\times10^{-23}$ [m]. Naturally, this condition was chosen arbitrarily. Otherwise, it is possible that one will never find an exact radius of the electron. In the case of the proton, the radius is also not known exactly.

6. CONCLUSIONS

The best way to obtain an experimentally verified value of the depth of space, W, of a gravitational funnel in the 4-th spatial dimension seems to be the light bending at the planet Jupiter. Although the planet has an extensive and strong magnetosphere, it does not have a radiant corona as the sun. The influence of the magnetosphere is small enough for accurate measurements. Thanks to ESA's GAIA mission, sufficient stellar data are now available, but they are still waiting to be evaluated for this special case of light diffraction.

COMPETING INTERESTS

Authors have declared that no competing interests exist.

REFERENCES

1. vonWeber S, vonEye A. Multiple weighted regression analysis of the curvature of a 3D Brane in a 4D Bulk Space under a Homogeneous Vector Field. InterStat. 2010; July.
Available:https://www.researchgate.net/publication/228586887_Multiple_Weighted_R

egression_Analysis_of_the_Curvature_of_a_3D_Brane_in_a_4D_Bulk_Space_under_a_Homogenous_Vector_Field
2. vonWeber S, vonEye A. Monte Carlo study of vector field-induced dark matter in a spiral galaxy. InterStat. 2011; August. (Link is broken. Please demand the PDF privately from the author)
3. vonWeber S, vonEye A. Error analysis of simulated einstein rings under the membrane paradigm. InterStat. 2013; October. (Link is broken. Please demand the PDF privately from the author)
4. vonWeber S, vonEye A. Geodetic Precession under the Paradigm of a Cosmic Membrane. Phys. Sci. Int. J. 2016;10(4):1-14.
DOI: WeberEye4
5. vonWeber S, vonEye A. Two-way and one-way vacuum speed of light under the membrane paradigm. Phys. Sci. Int. J. 2017;15(2):1-17. WeberEye5
6. vonWeber S, vonEye A. Dilation of Time and Newton's Absolute Time, Phys. Sci. Int. J. Vol. 2019;23(1):1-20.
WeberEye6
7. Onoochin V, vonWeber S. On the size of moving rigid bodies determined from conditions of equilibrium of ions in a crystalline lattice. In Einstein and Poincaré: The Physical Vacuum. Dvoeglazov VV, editor. Apeiron Montreal; 2006. ISBN 0-9732911-3-3.
Einstein and Poincare: the physical vacuum - PDF Free Download
8. Mueller E. De la réalité des nombres. Bull. Soc. Frib. Sc. Nat. 2014;103:83-90.
Available :https:De la réalité des nombres - e-periodica
9. Feynman/Leighton/Sands: Feynman - Vorlesungen über Physik, Oldenbourg Verlag; 1987.
10. Puthoff HE. Polarizable-vacuum approach to GR, Found. of Physics. 2002;32:6.
Puthoff 2002
11. Yarman T, Kholmetskii A, Arik M. Bending of light caused by gravitation: the same result via totally different philosophies; 2014.
Available :arXiv:1401.3110 [physics.gen-ph]
12. Shapiro II, Reasenberg RD, MacNeil PE, Goldstein RB, Brenkle JP, Cain DL, Komarek T, Zygielbaum AI, Cuddihy WF, Michael WHJr. The viking relativity experiment. J. of Geophys. R. 1977;82:4329.
DOI: 10.1029/js082i028p04329
Shapiro 1977
13. Althaus T. Cassini-huygens – Die erforschung des saturnsystems. In: *Sterne und Weltraum*. Spektrum der Wissenschaft Verlagsgesellschaft. Oktober 1997;S:838–847.
Cassini-Huygens – Die Erforschung des Saturnsystems
14. Bertotti B, Iess L, Tortora P. A test of general relativity using radio links with the Cassini spacecraft, letters to nature. Nature. 2003;425:374–376.
Available :https://www.nature.com/articles/nature01997
15. Stöcker H. Taschenbuch mathematischer Formeln. Verlag Harri Deutsch, ISBN 3-8171-1256-4; 1993.
16. Weinberg S. Gravitation and cosmology. Wiley; 1972.
17. Premadi P, Martel H, Matzner R. Light propagation in inhomogenous universes. I. Methodology and preliminary results. Ap J. 1998;493:10.
Available :https://arxiv.org/abs/astro-ph/9708129
18. Bruckman, W, Esteban, EP. An alternative calculation of light bending and time delay by a gravitational field. Am.J.Phys. 1993;61(8):750.
Available :https://ui.adsabs.harvard.edu/abs/1993AmJPh..61..750B/abstract
19. Dyson FW, Eddington AS, Davidson C. A determination of deflection of light, Philosophical Transactions of the Royal Society of London. Series A, Containing Papers of a Mathematical or Physical Character, Volume 220, pp. 291-333, 1920
Available :https://ui.adsabs.harvard.edu/abs/1920RSPTA.220..291D/abstract
20. Van Bienstock G. The relativity shift at the 1952 february 25 eclipse of the sun. Astronomical Journal. 1953;58:87-88.
DOI:10.1086/106825
21. Mattig W. Wenn die Sonne sich verfinstert. Physik in unsrer Zeit. 1999;4:S.153.
22. Schmutzer E. Grundlagen der Theoretischen Physik, Wiley 2005
23. Robertson DS, Carter WEr. Relativistic deflection of radio signals in the solar gravitational field measured with VLBI, Nature. 1984;310:572.
Available :https://ui.adsabs.harvard.edu/abs/1984Natur.310..572R/abstract
24. Fomalont E, Kopeikin S, Lanyi G, Benson J. Progress in measurements of the gravitational bending of radiowaves using

the vlba. The Astrophysical Journal. 2009;699(2).
Available :https://iopscience.iop.org/article/10.1088/0004-637X/699/2/1395
25. Prusti T, et al. The GAIA-mission, Astronomy&Astrophysics, A1, 595, (2016) p. 3-5.
Available :https://www.aanda.org/articles/aa/abs/2016/11/aa29272-16/aa29272-16.html
26. Abbas U, Bucciarelli B, Lattanzi MG. Differential astrometric framework for the Jupiter relativistic experiment with *Gaia.* MNRAS. 2019;485:1147–1156.
Available :https://arxiv.org/abs/1901.08903
27. Fomalont EB, Kopeikin SM. The measurement of the light deflection from jupiter: experimental results. Astrophys. J. 2003;598:704-711.
Available :https://arxiv.org/abs/astro-ph/0302294
28. Salah E. the radius of electron. Advances in Physics Theories and Applications. 2020;83.
DOI: 10.7176/APTA/83-07
29. Chinese Particle Data Group. Review of particle physics. Chinese Physics C. 2014;38(9):090001
Available :https://pdg.lbl.gov/2015/download/rpp2014-Chin.Phys.C.38.090001.pdf
30. Simulik V. What is the electron. Apeiron Montreal; 2005.
Available :http://library.uc.edu.kh/userfiles/pdf/42.What%20is%20the%20electron.pdf
31. Bagenal F. The magnetosphere of Jupiter: Coupling the equator to the poles Fran Bagenal_ Journal of Atmospheric and Solar-Terrestrial Physics. 2007;69:387–402.
Available :https://ui.adsabs.harvard.edu/abs/2007JASTP..69..387B/abstract

Peer-review history:
The peer review history for this paper can be accessed here:
https://www.sdiarticle4.com/review-history/70903